

# Phase behavior and critical activated dynamics of limited-valence DNA nanostars

Silvia Biffi<sup>a</sup>, Roberto Cerbino<sup>a</sup>, Francesca Bomboi<sup>b,c</sup>, Elvezia Maria Paraboschi<sup>a</sup>, Rosanna Asselta<sup>a</sup>, Francesco Sciortino<sup>b,1</sup>, and Tommaso Bellini<sup>a,1</sup>

<sup>a</sup>Department of Medical Biotechnology and Translational Medicine, Università degli Studi di Milano, I-20133 Milan, Italy; <sup>b</sup>Department of Physics, Sapienza, Università di Roma, I-00185 Rome, Italy; and <sup>c</sup>Department of Physics, Università degli Studi Roma Tre-Consortio Nazionale Interuniversitario per le Scienze Fisiche della Materia, I-00146 Rome, Italy

Edited by T. C. Lubensky, University of Pennsylvania, Philadelphia, PA, and approved August 6, 2013 (received for review March 14, 2013)

**Colloidal particles with directional interactions are key in the realization of new colloidal materials with possibly unconventional phase behaviors. Here we exploit DNA self-assembly to produce bulk quantities of “DNA stars” with three or four sticky terminals, mimicking molecules with controlled limited valence. Solutions of such molecules exhibit a consolution curve with an upper critical point, whose temperature and concentration decrease with the valence. Upon approaching the critical point from high temperature, the intensity of the scattered light diverges with a power law, whereas the intensity time autocorrelation functions show a surprising two-step relaxation, somehow reminiscent of glassy materials. The slow relaxation time exhibits an Arrhenius behavior with no signs of criticality, demonstrating a unique scenario where the critical slowing down of the concentration fluctuations is subordinate to the large lifetime of the DNA bonds, with relevant analogies to critical dynamics in polymer solutions. The combination of equilibrium and dynamic behavior of DNA nanostars demonstrates the potential of DNA molecules in diversifying the pathways toward collective properties and self-assembled materials, beyond the range of phenomena accessible with ordinary molecular fluids.**

DNA nanotechnology | limited valence colloids | critical behavior

In recent years, a strong effort has been devoted to introduce a new generation of micro- and nanocolloids interacting via strongly anisotropic forces. Anisotropic interactions can simply arise from a nonspherical particle shape or from more sophisticated physical and/or chemical patterning of the particle surface (1–7). An alternative strategy to produce complex nanoparticles is to exploit the self-assembly of DNA oligomers. The rational design of the DNA sequences enables guiding the association of multiple DNA strands into a rich variety of nanosized objects, such as geometrical figures, hollow capsules, and nanomachines, as well as more complex meso- and macroscopic structures (8–13). The selectivity of DNA binding can also be exploited to control the mutual interactions between the structures (14, 15), whereas the spontaneous assembly of DNA sequences enables producing large ensembles of particles. These properties make DNA a powerful tool to explore fundamental phenomena of soft matter and statistical physics, as indicated by previous studies of liquid-crystalline ordering and phase separations in solutions of short DNA oligomers (16–18). Here we exploit DNA self-assembly to experimentally address the phase behavior of particles interacting with specific valence, strength, and selectivity.

Colloidal particles with controlled valence are the next step toward the realization of new colloidal materials and phases dependent on the presence of a small number of bonds (1–7). Theoretical and numerical studies (19) predict that a solution of low-valence particles should exhibit phase coexistence—the colloidal analog of the vapor–liquid coexistence in simple liquids—but only at very small concentrations. The unstable region in the temperature–concentration ( $T$ – $c$ ) plane is expected to significantly shrink, with critical temperature  $T_c$  and critical concentration

$c_c$  decreasing and approaching zero as the valence is reduced. Indirect support to theoretical predictions comes from recent experiments (20), which have interpreted the irreversible aging dynamics of a synthetic clay as an equilibrium gelation process (21) by invoking an effective (although unknown) limited valence of the clay particles. However, despite these promising findings, the absence of a strategy for realizing bulk quantities of particles with reversible interactions and with controlled valence (1) has until now hampered the experimental investigation of the systematic dependence of the coexistence curve on the valence.

Here we focus on DNA molecules with valence  $f = 3$  and 4, the latter potentially reproducing on a colloidal length scale the behavior of silica and of other network-forming molecules like water (22). Particles are shaped as nanostars having  $f$  arms with sticky tips. At variance with DNA structures aimed at the formation of 2D and 3D crystals, which required a big effort in carefully determining the optimal location of the interacting sequences, the liquid–vapor transition is expected to be rather insensitive to the position of the sticky spots (23), giving us the benefit of basing our study on the simplest structures granting controlled valence. DNA nanostars are obtained by dissolving in water equimolar quantities of  $f$  distinct 49-base-long oligonucleotides. Sequences are designed to self-assemble around  $T_{sa} \approx 65$  °C, forming structures with  $f$  double-stranded arms of 20 bases each (Fig. 1 *A* and *B*). To enable angular flexibility between different arms, bases with no complementary partner were inserted

## Significance

**At atomic and molecular levels, particles interact via the immutable laws of quantum mechanics, whereas at nanoscopic and microscopic levels, interactions between colloidal particles can be determined by human design. We exploit DNA self-assembly to produce nanoscopic particles with a controlled number of interacting terminations, providing the particles with valence. Experimental investigation of the collective behavior of such colloids shows that reducing the number of interacting sites results in a significant shrinkage of the gas–liquid coexistence region, with critical parameters decreasing as the valence is reduced. We also observe an unconventional dynamic behavior in the proximity of the critical point. Such findings are relevant to answer fundamental physics issues and potentially to determine the stability region of new DNA-based materials.**

Author contributions: R.C., F.S., and T.B. conceived the study; S.B., R.C., R.A., and T.B. designed the sequences and the experiments; S.B. and E.M.P. characterized the DNA nanostars and measured the phase diagram; S.B. and F.B. performed the light scattering experiments; S.B., R.C., F.B., F.S., and T.B. analyzed data; and S.B., R.C., F.S., and T.B. wrote the paper.

The authors declare no conflict of interest.

This article is a PNAS Direct Submission.

<sup>1</sup>To whom correspondence may be addressed. E-mail: tommaso.bellini@uniroma1.it or francesco.sciortino@uniroma1.it.

This article contains supporting information online at [www.pnas.org/lookup/suppl/doi:10.1073/pnas.1304632110/-DCSupplemental](http://www.pnas.org/lookup/suppl/doi:10.1073/pnas.1304632110/-DCSupplemental).

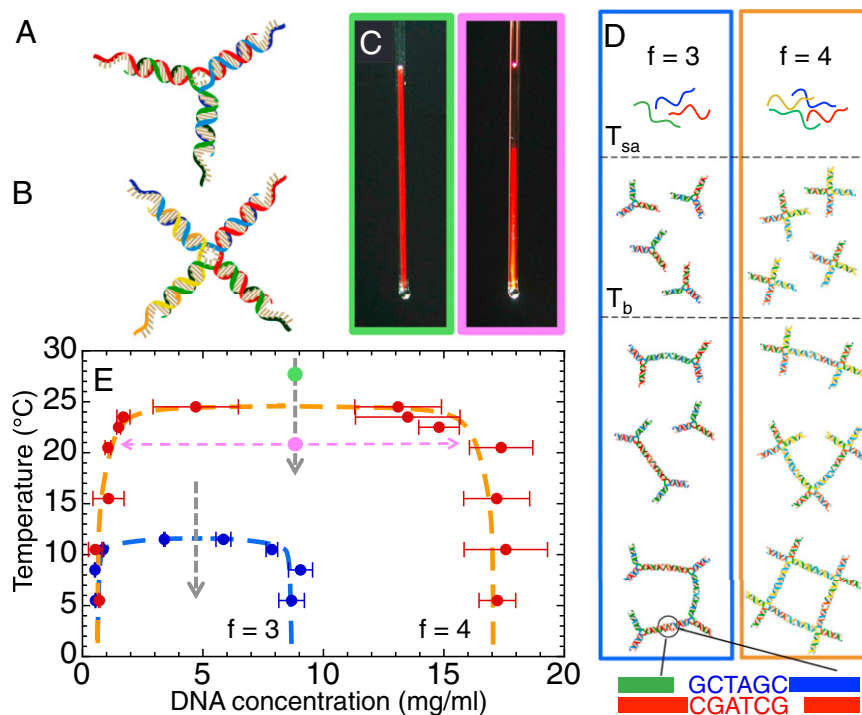


**Fig. 1.** Phase behavior of DNA nanostars with valence  $f=3$  and  $f=4$ . (A) The  $f=3$  and (B)  $f=4$  nanostars are formed by the self-assembly of three and four oligomers, respectively. Arm tips terminate with one sticky overhang each. (C) Fluorescent emission from a capillary tube containing a sample of EtBr-marked  $f=4$  nanostars photographed after the sample was centrifuged at two different  $T$  (as indicated by the green and magenta dots in E). At low-enough  $T$  (magenta-framed picture, *Right*), the system phase separates into DNA-rich and DNA-poor phases. (D) Above  $T_{sa} \approx 65$  °C, DNA is single stranded. For  $T < T_{sa}$ , single strands hybridize, leading to the self-assembly of stable  $f=3$  (blue frame, *Left*) and  $f=4$  (orange frame, *Right*) nanostars. For  $T > T_b \approx 42$  °C, nanostars are independent. Below  $T_b$ , interactions between sticky overhangs (see schematic at the bottom) promote the formation of clusters that grow progressively larger as  $T$  is lowered. (E) Experimentally determined consolution curve for nanostars with  $f=3$  (blue dots) and  $f=4$  (red dots). The  $f=3$  nanostars have a markedly reduced coexistence region with respect to  $f=4$  nanostars. The concentrations of the dense phases at low  $T$  correspond to nanostars molarities of 0.20 mM and 0.29 mM for  $f=3$  and  $f=4$ , respectively. As  $T$  is lowered from stable homogeneous conditions (green dot and C *Left*, green-framed picture) to a temperature within the consolution curve (magenta dot and C *Right*, magenta-framed picture) along the critical isochores (dashed gray arrows), the system phase separates into two coexisting phases whose concentration is indicated by the magenta tie line.

between the arm-forming sequences. Each arm terminates with an equal six-nucleotide-long overhang of sequence CGATCG. This self-complementary sequence promotes nanostars association via Watson–Crick pairing of the overhangs of close-by structures. We used the same overhang sequence for  $f=3$  and  $f=4$  nanostars to provide identical interaction strength in structures of different  $f$ . Details about sequences, sample preparation, nanostars assembly, and energy evaluations are given in *Materials and Methods* and in *SI Text*. Because the binding between sticky overhangs is stronger than all other interparticle interactions (excluded volume, van der Waals, electrostatic), DNA nanostars provide an optimal model for highlighting the role of the valence. Similar DNA nanostars were studied by Luo and coworkers (24, 25) to investigate their gelation in the presence of enzymatic catalysis. We operate in the absence of any enzymes to benefit the reversibility of the DNA interaction and systematically investigate the equilibrium phase behavior.

We studied the phase diagram by characterizing the behavior of samples prepared at different DNA nanostars concentrations ( $c_{DNA}$ ). We found a large  $T$  interval in which nanostars with desired valence were well formed but weakly interacting (Fig. 1D), coherently with the expectation that the binding between overhangs of different nanostars should start becoming relevant at  $T_b \approx 42$  °C  $\ll T_{sa}$ . In this range of  $T$ , samples remained homogeneous with no detectable sign of a phase separation. Upon cooling enough, all investigated samples were found to phase separate into coexisting small droplets, providing evidence of a phase separation process between two phases differing into

particle concentration. To properly evaluate the coexisting concentrations, each sample was centrifuged at a fixed  $T$  for several hours. For each  $c_{DNA}$  we found a temperature  $T_s$  such that samples centrifuged at  $T < T_s$  developed a clear meniscus, whereas for  $T > T_s$  no sign of a phase separation was detected (Fig. 1C). The measurement of DNA concentration via UV absorption in the two phases (*SI Text*) allowed us to determine the  $T$  dependence of the concentration of the coexisting phases for both  $f=3$  and  $f=4$  nanostars and to build the phase diagram reported in Fig. 1E.

The range of  $c_{DNA}$  where separation takes place is rather limited and decreases from  $f=4$  to  $f=3$ . The concentration of the dense phase is comparable to the concentration of regular networks in which DNA nanostars are fully bonded with  $f$  neighbors each. Indeed, simple geometrical considerations indicate that the DNA concentration of such networks is rather small and strongly depends on the nanostar valence. A diamond lattice formed by  $f=4$  nanostars in which all paired arms were perfectly aligned would have a density of  $c_{DNA} \approx 13.3$  mg/mL (see *SI Text* for more detail). Our findings thus indicate that the dense fluid phase has indeed a density comparable to the fully bonded network state. We also find that the critical temperature  $T_c$  decreases with decreasing  $f$ , again in agreement with qualitative arguments that take into account the  $T$  dependence of the DNA binding free energy (*SI Text*). These considerations, together with the agreement of our results with theoretical predictions (19), indicate that the dependence of the coexistence

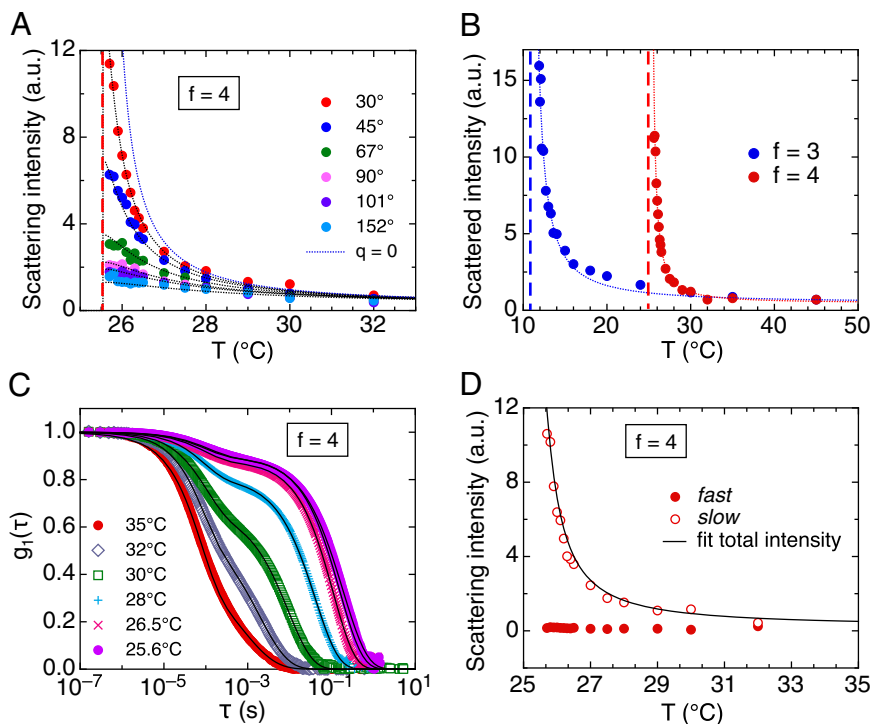


**Fig. 2.** Pretransitional behavior of  $f=4$  DNA nanostars along the critical isochore. (A) Scattered intensity measured as a function of  $T$  at various scattering angles. The scattering angles and the corresponding scattering vectors explored in this experiments are  $30^\circ$  ( $q = 8.15 \mu\text{m}^{-1}$ ),  $45^\circ$  ( $q = 12.1 \mu\text{m}^{-1}$ ),  $68^\circ$  ( $q = 17.6 \mu\text{m}^{-1}$ ),  $90^\circ$  ( $q = 22.3 \mu\text{m}^{-1}$ ),  $101^\circ$  ( $q = 24.3 \mu\text{m}^{-1}$ ), and  $152^\circ$  ( $q = 30.6 \mu\text{m}^{-1}$ ). (B)  $T$  dependence of the scattered intensity measured at  $30^\circ$  (full symbols) for both  $f=3$  and  $f=4$  systems. Dotted lines in A and B are the best fit by the Lorentzian function in Eq. 1 (dotted lines). Dashed vertical lines indicate  $T_c$  as determined by the best fit. Scattered intensities relative to the  $f=4$  structures have been divided by a factor of 2 to make them overlap with  $f=3$  data at high  $T$ . (C) Field correlation functions  $g_1(\tau)$  measured at  $90^\circ$  in the  $f=4$  system for various  $T$  (symbols). Data are fitted to a sum of two stretched exponentials (lines). (D) Scattering intensity associated to the fast and slow contributions of  $g_1$  at scattering angle  $30^\circ$ . The line is the fit to the total scattered intensity reported in B.

region from the particles valence that we observe with the DNA nanostars is universal for limited valence systems.

The experimentally determined consolution curve necessarily terminates, at high  $T$ , in a critical point ( $c_c, T_c$ ) marking the divergence of DNA concentration fluctuations. To characterize such critical behavior we investigated amplitude and dynamics of the pretransitional concentration fluctuations by preparing samples at  $c_c \approx 4.5 \text{ mg/mL}$  ( $f=3$ ) and  $c_c \approx 9.0 \text{ mg/mL}$  ( $f=4$ ) and lowering  $T$  to approach  $T_c$ . Measurements were done via static and dynamic light-scattering experiments for six different angles covering the wave vector range  $8.2 \mu\text{m}^{-1} < q < 30.5 \mu\text{m}^{-1}$ . This experimental approach takes advantage of the large refractive index of DNA, enabling an effective detection of concentration fluctuations.

Fig. 2A shows the intensity scattered by the solutions of  $f=4$  nanostars along the critical isochore at various scattering angles, ranging from  $30^\circ$  to  $152^\circ$ . All data can be simultaneously fitted by a Lorentzian shape

$$I(q) = \frac{I_L(0)}{1 + q^2 \xi^2} + I_{nc}, \quad [1]$$

which expresses the dependence of the susceptibility on  $T$  and on the scattering wave vector  $q$  in the critical region. In Eq. 1,  $I_L(0)$  diverges as  $I_L(0) = I_0(T/T_c - 1)^{-\gamma}$ , whereas  $\xi$  is the correlation length, diverging as  $\xi = \xi_0(T/T_c - 1)^{-\nu}$ .  $I_0$  and  $\xi_0$  provide the reference values of the critical scattering intensity and of the thermal correlation length far from the critical point.  $I_{nc}$  accounts for the (small) noncritical component of the scattered intensity. The appropriate Ising exponents are  $\gamma = 1.237$  and  $\nu = 0.630$  (26). The simultaneous best fit of the scattered intensity at all measured  $T$

and  $q$  values (lines in Fig. 2A) provides a robust estimate for the four fit parameters  $T_c$ ,  $\xi_0$ ,  $I_0$ , and  $I_{nc}$ . Analogous analysis has been performed on solutions of  $f=3$  nanostars (SI Text). The resulting values for the critical temperatures are  $T_c = 11.6 \pm 0.1^\circ\text{C}$  and  $T_c = 25.5 \pm 0.1^\circ\text{C}$  for  $f=3$  and  $f=4$ , respectively (vertical lines in Fig. 2B). The best fit yields  $\xi_0 = 3.2 \text{ nm}$  and  $\xi_0 = 1.9 \text{ nm}$  for  $f=3$  and  $f=4$ , respectively. These values are in the range of the hydrodynamic radius of the nanostar ( $\approx 4.5$  and  $4.7 \text{ nm}$  for  $f=3$  and  $f=4$ ), and reflect the different critical density of the two systems, smaller in the case of  $f=3$ . The marked increase of the intensity scattered by both  $f=3$  and  $f=4$  nanostars upon lowering  $T$ , compared in Fig. 2B for a scattering angle equal to  $30^\circ$ , our smallest accessible scattering angle, provides evidence of the growth of critical concentration fluctuations. To the best of our knowledge, no other example of critical behavior in DNA solutions was previously reported.

Though the  $I(q)$  divergence in Fig. 2A and B follows expectations, the dynamic behavior is richer than anticipated. The theory of dynamic critical phenomena predicts an exponential decay of the correlation function and a single characteristic time diverging as power law upon approaching the critical point, the so-called “critical slowing down.” Instead, as the critical point is approached, the field correlation functions  $g_1(\tau)$  become characterized by a two-step relaxation process (Fig. 2C), with the clear insurgence of a plateau whose height (the so-called “nonergodicity factor” in glass physics) (27) increases on cooling. All correlation functions can be well fitted to the sum of two stretched exponentials

$$g_1(\tau) = A_F \cdot \exp\left[-\left(\frac{\tau}{\tau_F}\right)^{\beta_F}\right] + A_S \cdot \exp\left[-\left(\frac{\tau}{\tau_S}\right)^{\beta_S}\right], \quad [2]$$

where  $A_F$  and  $A_S$ ;  $\tau_F$  and  $\tau_S$ ; and  $\beta_F$  and  $\beta_S$  are the amplitudes (with  $A_F + A_S = 1$ ), characteristic times, and stretching exponents of the fast and slow components, respectively.

The clear separation in two fast and slow components allows us to decouple the contribution of the two processes to the static scattering, by weighting the total intensity with the two amplitudes  $A_F$  and  $A_S$ . The result of such a procedure, shown in Fig. 2D, indicates that the critical growth of the scattered intensity is entirely associated with the slow decay.

As  $T$  decreases, the two characteristic times  $\tau_F$  and  $\tau_S$  behave very differently (Fig. 3A). At high  $T$ , the dynamics is the one expected for independent, free-diffusing DNA nanostars, with a single exponential decay process having a characteristic time coherent to the time expected for the nanostar radius. As  $T$  is lowered, such relaxation develops continuously into the fast component, with the stretching exponent decreasing (Fig. 3B) and  $\tau_F$  changing only very mildly, not unlike what is expected for the  $T$  dependence of free diffusion. Quite different is the behavior of  $\tau_S$ , which slows down more than three orders of magnitude in a continuous fashion. Fig. 3C shows that  $\tau_S$  behaves as an Arrhenius-activated process  $\tau_S = \tau_0 \exp(\Delta G/k_B T)$ , where  $\tau_0$  is the characteristic time found in the limit of high  $T$ . By fitting the slope of  $\ln(\tau_S)$  vs.  $1/T$ , we determined  $\Delta H$ , the enthalpic component of  $\Delta G$ . We find  $\Delta H = 82$  kcal/mol and  $\Delta H = 120$  kcal/mol for  $f = 3$  and  $f = 4$  nanostars, respectively. These values correspond to  $\sim 2.0$  and  $3.0$  times the enthalpic component expected for the binding of the sticky overhangs (SI Text). The entropic component associated with slow relaxation is instead less immediately accessible, because to extract it, it is necessary to have an independent estimate of  $\tau_0$ . A simple choice is to assume  $\tau_0 = \tau_F$ . Under this assumption, we obtain  $\Delta S = 266$  cal/(mol K) and  $\Delta S = 386$  cal/(mol K) for the  $f = 3$  and  $f = 4$  systems, respectively. These values correspond, respectively, to  $\sim 2.0$  and  $3.0$  times the entropic component expected for the binding of the sticky overhangs (SI Text), in line with that obtained for the enthalpic component. This analysis indicates that as critical fluctuations start to develop, ergodicity is achieved via the

breaking of bonds between nanostars. Indeed, density fluctuations can be viewed as the buildup of networks of bonded nanostars. Local disruptions of bonds enables the readjustment of the network either through nanostars “evaporating” away from the network and reconnecting elsewhere or through the rearrangements of network portions made flexible by the opening of bonds. The kinetics of this process is intrinsically limited by the rate of unbinding events, easily spanning into the millisecond regime (28–30) (see SI Text for further discussion).

Our results show that the characteristic time of the slow process, despite being associated with critical density fluctuations, has a temperature dependence with no sign of the power-law divergence expected for critical slowing down. We interpret the dominance of the activated dynamics over the conventional slowing down as a consequence of the long lifetime of the bonds between DNA structures, larger than the time necessary for free structures to diffuse over distances comparable to  $\xi$ . In this condition, the decay of density correlations hinges on the restructuring of the large clusters, and it is thus determined by the bond lifetime. As illustrated in Fig. 3D, the critical slowing down is in this system probably constrained in a narrow  $T$  interval around  $T_c$ , where the collective diffusional time across  $\xi$  becomes larger than the time required for activated bond rupture. The simple estimates in Fig. 3D indicate that such an interval is too narrow to be experimentally accessed with our instrumentation.

The breakdown of dynamic universality here observed has strong analogies with the behavior of polymeric solutions in the proximity of their critical demixing point. As in the present case of DNA nanostars, polymeric solutions also feature a double relaxation and follow an unconventional critical dynamics as the critical point is approached (31, 32). In both systems, the dynamics close to the critical point is modified by the presence of slow microscopic mechanical relaxations that overshadow the collective behavior. This unusual phenomenon is explained by dynamic coupling of critical concentration fluctuations with an additional slow viscoelastic mode intrinsic to polymer solutions. Such anomalous kinetics may extend in a large range of  $T$ , including temperatures close to  $T_c$ , where the critical behavior is typically expected. As a result, the cross-over to the conventional critical slowing down is pushed to temperatures so close to  $T_c$  to be practically undetectable. Similar coupling between a critical mode and a slow relaxational mode has been proposed as a universal feature distinctive to mixtures whose components have strong dynamic asymmetries, including polymer solutions, protein solutions, and colloidal dispersions (33). In the case of DNA nanostars, the noncritical dynamics result from a subtle combination of selectivity, interaction energy, and lifetime, which can all be very finely tuned using DNA strands with different sequence and length, offering powerful handles for the exploration of this class of dynamic phenomena.

Our results demonstrate that DNA structures are unique particles for investigating the phase behavior of systems in which it is possible to tune binding selectivity (via the DNA sequence), strength of interaction (via the DNA length), and valence. Key in this application is the strong temperature dependence of the DNA duplex binding strength, which enables exploring a wide range of bond energies and bond lifetimes, as no other model system does. We foresee that a large variety of topics in statistical physics can be experimentally addressed through the use of DNA supermolecules, including reentrant behaviors induced by competitive interactions (34, 35), higher-order network–network critical points (36), and arrested states of matter (glasses and gels) (27). In the specific case of limited valence structures here discussed, our results set the basis to predict the thermal and kinetic stability of self-assembled DNA hydrogels (25), a finding with relevant implications in the design of commercial complex fluids with tailored properties.

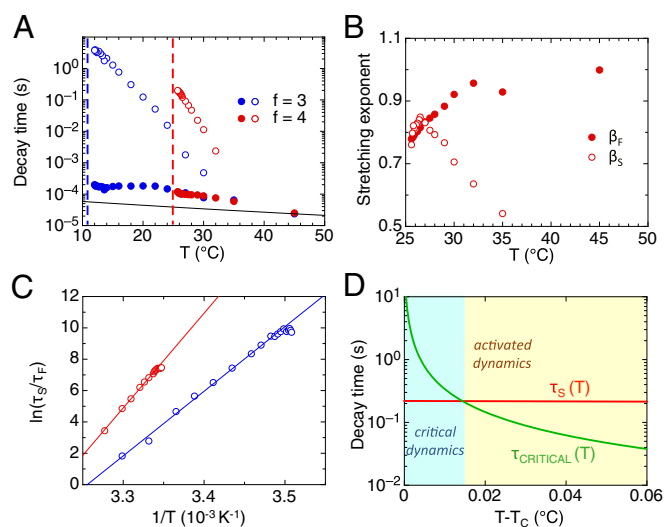


**Fig. 3.** Dynamic behavior of  $f = 3$  and  $f = 4$  DNA nanostars along the critical isochore. (A)  $T$  dependence of the slow and fast decay times. The black line shows the expected  $T$  dependence of the diffusive  $\tau$  for independent nanostars. (B)  $T$  dependence of the stretching exponent for the fast and for the slow components. (C)  $\ln(\tau_S/\tau_F)$  plotted as function of  $1/T$  and fitted by an Arrhenius law. (D) Comparison, in a narrow  $T$  interval close to  $T_c$ , of the extrapolated Arrhenius  $T$  dependence observed for  $\tau_S$  for the  $f = 4$  DNA nanostars with the correlation times expected on the basis of the critical slowing down (SI Text).

## Materials and Methods

**Sample Preparation.** DNA sequences (*SI Text*) were purchased from Primm S.p.a. with PAGE purification. Desalting was performed using Illustra NAP-10 columns (GE Healthcare). The  $f=3$  and  $f=4$  nanostars were formed by mixing equimolar quantities of the three and four strands, respectively, involved in the structures.

DNA was dissolved in electrolyte solution having ionic strength 35 mM NaCl in the case of  $f=3$  and of 25 mM NaCl in the case of  $f=4$ . Ionic strengths were chosen to yield similar ionic conditions in the two samples despite the difference in the DNA critical concentration, assuming that each phosphate dissociates one cation. The resulting ionic strength for both systems is  $\sim 50$  mM NaCl. Two different cells were prepared: (i) to measure the phase diagram, glass microcapillary pipettes (Kimble Glass Inc. microcapillary pipettes,  $20 \mu\text{L} \pm 0.5\%$ ) were filled with  $7\text{--}8 \mu\text{L}$  of solution and flame sealed at both ends; (ii) to perform dynamic light-scattering measurements, NMR cylindrical, borosilicate glass tubes (inner diameter = 2.4 mm) were filled with  $\sim 50 \mu\text{L}$  of sample and topped with  $\sim 30 \mu\text{L}$  of silicon oil to avoid evaporation and condensation on the tube walls. After flame sealing, the solutions were kept at  $90^\circ\text{C}$  for  $\sim 20$  min and slowly cooled to room temperature in  $\sim 3$  h. We verified the formation of the nanostars by further diluting the samples in 50 mM NaCl electrolyte solutions, and inspected them via gel electrophoresis (*SI Text*). This analysis confirmed that more than 92% of the sequences were always bound into the desired trimeric and tetrameric structures.

**Determination of the Phase Diagram.** To determine the phase diagram, we cooled identically prepared and previously annealed capillaries at the target temperatures, at which we centrifuged them for  $\sim 4$  h at  $3,000 \times g$  to speed

up macroscopic phase separation. We cut each capillary in sections, and for each of them we determined the DNA concentration by measuring the absorbance at 260 nm using a Thermo Scientific NanoDrop 1000 Spectrophotometer. In solutions of  $f=4$  nanostars, the difference in density between the two coexisting phases was sufficiently large to identify the meniscus by naked eye. By contrast, because in solution of  $f=3$  nanostars the visibility of the meniscus was low, we doped selected samples with ethidium bromide with about one fluorophore per DNA structure. Such samples, similar to the one shown in Fig. 1C for  $f=4$  structures, provided a clear visualization of the meniscus and were used to guide the cutting process.

**Light-Scattering Measurements.** Static and dynamic light-scattering measurements were performed on a ST100 SciTech Instruments apparatus, customized to measure samples with small volume. Measurements were performed with a 532-nm solid-state laser source at various scattering angles:  $\theta = 30^\circ, 45^\circ, 68^\circ, 90^\circ, 101^\circ, 152^\circ$ . Measurements were performed above the critical point, by first thermalizing the sample at  $45^\circ\text{C}$  and upon progressively cooling. After changing temperature, the sample was allowed to thermalize for 2 h before measuring. At each  $T$  we performed three identical sets of simultaneous static and dynamic light-scattering experiments separated in time by 2 h.

**ACKNOWLEDGMENTS.** For helpful discussions, F.B. and F.S. thank F. Bordini and P. Filetici, and T.B., S.B., and R.C. thank M. Salina, M. Buscaglia, V. Trappe, and V. Rimoldi. We acknowledge support from the PRIN program of the Ministero dell'Istruzione, dell'Università e della Ricerca, Initial Training Network-Comploids, and European Research Council Grant Agreement 226207 (PATCHYCOLLOIDS).

- Wang Y, et al. (2012) Colloids with valence and specific directional bonding. *Nature* 491(7422):51–55.
- Glotzer SC, Solomon MJ (2007) Anisotropy of building blocks and their assembly into complex structures. *Nat Mater* 6(8):557–562.
- Jackson AM, Myerson JW, Stellacci F (2004) Spontaneous assembly of subnanometre-ordered domains in the ligand shell of monolayer-protected nanoparticles. *Nat Mater* 3(5):330–336.
- Yi G, et al. (2004) Colloidal clusters of silica or polymer microspheres. *Adv Mater* 16(14):1204–1208.
- Kraft DJ, Groenewold J, Kegel WK (2009) Colloidal molecules with well-controlled bond angles. *Soft Matter* 5(20):3823–3826.
- Chen Q, Bae SC, Granick S (2011) Directed self-assembly of a colloidal kagome lattice. *Nature* 469(7330):381–384.
- Sacanna S, Pine DJ (2011) Shape-anisotropic colloids: Building blocks for complex assemblies. *Curr Opin Colloid Interface Sci* 16(2):96–105.
- Bellini T, Cerbino R, Zanchetta G (2012) DNA-based soft phases. *Top Curr Chem* 318: 225–279.
- Liu D, Park SH, Reif JH, LaBean TH (2004) DNA nanotubes self-assembled from triple-crossover tiles as templates for conductive nanowires. *Proc Natl Acad Sci USA* 101(3): 717–722.
- Liu H, He Y, Ribbe AE, Mao C (2005) Two-dimensional (2D) DNA crystals assembled from two DNA strands. *Biomacromolecules* 6(6):2943–2945.
- Zheng J, et al. (2009) From molecular to macroscopic via the rational design of a self-assembled 3D DNA crystal. *Nature* 461(7260):74–77.
- Wei B, Dai M, Yin P (2012) Complex shapes self-assembled from single-stranded DNA tiles. *Nature* 485(7400):623–626.
- Maye MM, Nykypanchuk D, Cuisinier M, van der Lelie D, Gang O (2009) Stepwise surface encoding for high-throughput assembly of nanoclusters. *Nat Mater* 8(5): 388–391.
- Seeman NC (2003) DNA in a material world. *Nature* 421(6921):427–431.
- Condon A (2006) Designed DNA molecules: principles and applications of molecular nanotechnology. *Nat Rev Genet* 7(7):565–575.
- Nakata M, et al. (2007) End-to-end stacking and liquid crystal condensation of 6–20 base pair DNA duplexes. *Science* 318(5854):1276–1279.
- Zanchetta G, Nakata M, Buscaglia M, Bellini T, Clark NA (2008) Phase separation and liquid crystallization of complementary sequences in mixtures of nanoDNA oligomers. *Proc Natl Acad Sci USA* 105(4):1111–1117.
- Bellini T, et al. (2012) Liquid crystal ordering as evidence for the structured self-assembly of random-sequence DNA oligomers. *Proc Natl Acad Sci USA* 109:1110–1115.
- Bianchi E, Largo J, Tartaglia P, Zaccarelli E, Sciortino F (2006) Phase diagram of patchy colloids: towards empty liquids. *Phys Rev Lett* 97(16):168301–168304.
- Ruzicka B, et al. (2011) Observation of empty liquids and equilibrium gels in a colloidal clay. *Nat Mater* 10(1):56–60.
- Zaccarelli E (2007) Colloidal gels: Equilibrium and non-equilibrium routes. *J Phys Condens Matter* 19(32):323101.
- Sciortino F (2007) Gel-forming patchy colloids and network glass formers: Thermodynamic and dynamic analogies. *Eur Phys J B* 64:505–509.
- Bianchi E, Tartaglia P, Zaccarelli E, Sciortino F (2008) Theoretical and numerical study of the phase diagram of patchy colloids: ordered and disordered patch arrangements. *J Chem Phys* 128(14):144504.
- Li Y, et al. (2004) Controlled assembly of dendrimer-like DNA. *Nat Mater* 3(1):38–42.
- Roh YH, Ruiz RCH, Peng S, Lee JB, Luo D (2011) Engineering DNA-based functional materials. *Chem Soc Rev* 40(12):5730–5744.
- Pelissetto A, Vicari E (2002) Critical phenomena and renormalization-group theory. *Phys Rep* 368(6):549–727.
- Binder K, Kob W (2005) *Glassy Materials and Disordered Solids: An Introduction to Their Statistical Mechanics* (World Scientific, Singapore).
- Howorka S, Movileanu L, Braha O, Bayley H (2001) Kinetics of duplex formation for individual DNA strands within a single protein nanopore. *Proc Natl Acad Sci USA* 98(23):12996–13001.
- Woodside MT, et al. (2006) Nanomechanical measurements of the sequence-dependent folding landscapes of single nucleic acid hairpins. *Proc Natl Acad Sci USA* 103(16):6190–6195.
- Cisse II, Kim H, Ha T (2012) A rule of seven in Watson-Crick base-pairing of mismatched sequences. *Nat Struct Mol Biol* 19(6):623–627.
- Tanaka H, Nakanishi Y, Takubo N (2002) Nonuniversal nature of dynamic critical anomaly in polymer solutions. *Phys Rev E Stat Nonlin Soft Matter Phys* 65(2 Pt 1): 021802.
- Kostko AF, Anisimov MA, Sengers JV (2002) Dynamic crossover to tricriticality and anomalous slowdown of critical fluctuations by entanglements in polymer solutions. *Phys Rev E Stat Nonlin Soft Matter Phys* 66(2 Pt 1):020803.
- Tanaka H (2000) Viscoelastic phase separation. *J Phys Condens Matter* 12(15):R207.
- Russo J, Tavares JM, Teixeira PIC, Telo da Gama MM, Sciortino F (2011) Reentrant phase diagram of network fluids. *Phys Rev Lett* 106(8):085703.
- Angioletti-Uberti S, Moggetti BM, Frenkel D (2012) Re-entrant melting as a design principle for DNA-coated colloids. *Nat Mater* 11(6):518–522.
- Hsu CW, Largo J, Sciortino F, Starr FW (2008) Hierarchies of networked phases induced by multiple liquid-liquid critical points. *Proc Natl Acad Sci USA* 105(37): 13711–13715.